

Investigation on the $^{48}\text{Ca}+^{249-252}\text{Cf}$ reactions synthesizing isotopes of the 118 superheavy element

G. Mandaglio^{1,2,3}, G. Giardina^{2,3}, A. K. Nasirov^{4,5}, and A. Sobiczewski⁶
¹ *Centro Siciliano di Fisica Nucleare e Struttura della Materia, 95125 Catania, Italy*
² *Dipartimento di Fisica dell'Università di Messina, 98166 Messina, Italy*
³ *Istituto Nazionale di Fisica Nucleare, Sezione di Catania, 95123 Catania, Italy*
⁴ *Joint Institute for Nuclear Research, 141980 Dubna, Russia*
⁵ *Institute of Nuclear Physics, 100214, Tashkent, Uzbekistan*
⁶ *National Centre for Nuclear Research, Hoża 69, 00-681 Warsaw, Poland*
(Dated: Today)

The study of the $^{48}\text{Ca}+^{249,250,251,252}\text{Cf}$ reactions in a wide energy interval around the external barrier has been achieved with the aim of investigating the dynamical effects of the entrance channel via the ^{48}Ca induced reactions on the $^{249-252}\text{Cf}$ targets and to analyze the influence of odd and even neutron composition in target on the capture, quasifission and fusion cross sections. Moreover, we also present the results of the individual evaporation residue excitation functions obtained from the de-excitation cascade of the various even-odd and even-even $^{297-300}118$ superheavy compound nuclei reached in the studied reactions, and we compare our results of the $^{294}118$ evaporation residue yields obtained in the synthesis process of the $^{48}\text{Ca}+^{249,250}\text{Cf}$ reactions with the experimental data obtained in the $^{48}\text{Ca}+^{249}\text{Cf}$ experiment carried out at the Flerov Laboratory of Nuclear Reactions of Dubna.

PACS numbers: 25.70.Jj, 25.70.Gh, 25.85.-w

I. INTRODUCTION

In the last decade experiments were performed by using the ^{48}Ca beam against the ^{243}Am , $^{245,248}\text{Cm}$, ^{249}Bk and ^{249}Cf actinide targets (see Refs. [1–3]) in order to synthesize $Z=115,116,117$, and 118 superheavy elements, respectively, and to explore their characteristics. The possibility of obtaining the heaviest superheavy elements $^{302}119$ and $^{305}120$ by using the ^{48}Ca beam in the $^{48}\text{Ca}+^{254}\text{Es}$ and $^{48}\text{Ca}+^{257}\text{Fm}$ reactions, respectively is restricted by difficulties in obtaining a thick enough of ^{254}Es and ^{257}Fm actinide targets because the other Es and Fm isotopes are radioactive with shorter lifetimes. Therefore, in order to reach heavier superheavy elements (SHE), the beams heavier than ^{48}Ca (as for example ^{50}Ti , ^{54}Cr , ^{58}Fe , ^{64}Ni , and other heavier projectiles) against the above-mentioned actinide targets should be used. But, unfortunately, the evaporation residue (ER) cross sections decreases strongly by decreasing the charge (mass) asymmetry of reactants in the entrance channel. This is connected with the strong hindrance to formation of compound nucleus due to the dominant role of the quasifission process which competes with complete fusion. Quasifission is the decay of the formed dinuclear system (DNS) into two fissionlike fragments after the charge and/or mass exchange between its components without reaching the compound nucleus stage. The capture events that survive quasifission populate the complete fusion formation from which the deformed mononucleus may reach the statistically equilibrated shape of compound nucleus (CN). Another hindrance to formation of compound nucleus appears in collisions with large impact parameter-orbital angular momentum. Although DNS can survive against quasifission at large values of

angular momentum $L = \ell\hbar$ and it should be transformed into complete fusion, the mononucleus still not statically equilibrated can split into two fragments (fast fission process) if the fission barrier of this nuclear system disappears for high values of ℓ ($B_f(\ell > \ell_f) = 0$). Therefore, the fast fission process is present in reactions only at high angular momentum values ($\ell > \ell_f$, where ℓ_f is a characteristic value for each nucleus), while the quasifission process takes place at all ℓ values contributing to the capture reaction.

The first experiment which were performed at Flerov Laboratory of Nuclear Reaction of Joint Institute for Nuclear Reaction ($^{58}\text{Fe}+^{244}\text{Pu}$ [4]) and at GSI of Darmstadt ($^{64}\text{Ni}+^{238}\text{U}$ and $^{54}\text{Cr}+^{248}\text{Cm}$ [5], and $^{50}\text{Ti}+^{249}\text{Cf}$ [6]) to explore the synthesis of the $Z=120$ superheavy element did not identify any event of synthesis of the expected superheavy element. In our previous papers (see Refs. [7, 8]), we presented results of calculation on the above-mentioned reactions which could lead to the $Z=120$ superheavy element, but we found values of the evaporation residue cross sections lower than 0.1 pb. Predictions of other authors are approximately near this value [9–13]. Therefore, it is necessary to improve the experimental conditions in order to be able to reach measurements of cross sections of the order of fb. The dominant role of the quasifission process in reactions with massive nuclei is connected by the increase of the intrinsic fusion barrier depending on the shell structure of interacting nuclei and rotational energy of DNS which is formed at the given beam energy and orbital angular momentum in the entrance channel. Moreover, due to the fast fission process taking place at high orbital angular momentum values of the complete fusion system and the nearly fusion-fission process of excited and rotating compound nucleus, the possibility to synthesize in future superheavy elements

with $Z > 120$ by very massive nuclei reactions appears a very difficult task. We presented and discussed our results in Refs. [14, 15] about such perspectives.

The aim of this paper is to study four reactions induced by ^{48}Ca on the $^{249-252}\text{Cf}$ targets in order to analyze the effect of mass number and structure properties of nuclei in the entrance channel on the capture, quasifission, and complete fusion processes. For that we compare the capture, quasifission, and fusion cross sections for these considered reactions in order to analyze the influence of the odd or even neutrons present in target on the above-mentioned cross sections. The study and comparison of such cross sections allows us to reveal the sensitivity of the model and results on the dynamical effects of the entrance channel, while the determination and analysis of the evaporation residue cross sections for the four reactions reveal the influence of the different structure of the formed $^{297-300}118$ superheavy compound nuclei in the $^{48}\text{Ca}+^{249-252}\text{Cf}$ reactions with different neutron rich targets. Such reactions can be expected to occur in one, exceptional experiment, which could be performed to be performed in a near future. Its specific character should consist in the use of a target which is a mixture of the isotopes $^{249-252}\text{Cf}$. The amount of ^{252}Cf (which has a relatively short half-life) in the target is expected to be very small, but the percentage of the other are thought to be large and comparable with each other.

In Sect. II we present and analyze the results of the capture, quasifission, and fusion cross sections. In Sect. III we analyze excitation functions of the evaporation residue (ER) after few neutrons emission only from the formed compound nucleus (CN). Moreover, we compare our results for the $^{294}118$ residue nucleus which was synthesized in the $^{48}\text{Ca}+^{249,250}\text{Cf}$ reactions after evaporation of 3 and 4 neutrons from the $^{297}118$ and $^{298}118$ compound nuclei, respectively, with the experimental data concerning identification of $^{294}118$ superheavy nucleus observed in the $^{48}\text{Ca}+^{249}\text{Cf}$ experiment reported in Ref. [16]. The conclusions are presented in Sect. IV.

II. RESULTS OF THE CAPTURE, QUASIFISSION, AND FUSION CROSS SECTIONS

The evaporation residue formation, fusion-fission, quasifission and fast fission events take place if capture of projectile-nucleus by target-nucleus occurs after full momentum transfer due to the friction in relative motion and presence of potential well in nucleus-nucleus interaction.

In this work the capture probability is determined by solving the equations of radial motion, surface vibration of ^{48}Ca , and orbital angular momentum as in Refs. [7,

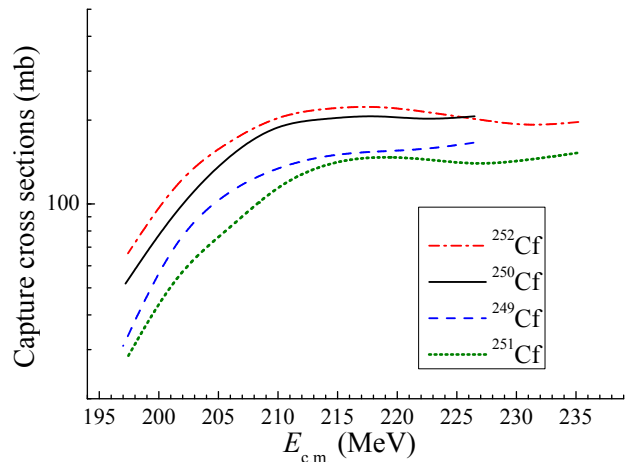


FIG. 1. (Color online) Comparison of the capture cross sections for the $^{48}\text{Ca}+^{249-252}\text{Cf}$ reactions.

8, 17, 18]:

$$F(R) = \mu(R, \alpha_T) \ddot{R} + \gamma_R(R, \alpha_T) \dot{R}, \quad (1)$$

$$F(R, \alpha_T) = -\frac{\partial V(R, \beta_i, \alpha_T)}{\partial R} - \dot{R}^2 \frac{\partial \mu(R)}{\partial R}, \quad (2)$$

$$F_{\beta_i}(R) = D_{\beta_i} \ddot{\beta}_i(t) + \gamma_{\beta}(R) \dot{\beta}_i(\alpha_T, t) + C_{\beta_i}^2 \beta_i, \quad (3)$$

$$F_{\beta}(R) = -\frac{\partial V(R, \beta_i, \alpha_T)}{\partial \beta_i}, \quad (4)$$

$$\begin{aligned} \frac{dL}{dt} &= \gamma_{\theta}(R, \alpha_T) R \times \\ &\times \left(\dot{\theta} R - \dot{\theta}_1 R_{1eff} - \dot{\theta}_2 R_{2eff} \right), \end{aligned} \quad (5)$$

$$L_0 = J_R(R, \alpha_T) \dot{\theta} + J_1 \dot{\theta}_1 + J_2 \dot{\theta}_2, \quad (6)$$

$$\begin{aligned} E_{\text{rot}} &= \mu(R, \alpha_T) \dot{R}^2 / 2 + \frac{J_R(R, \alpha_T) \dot{\theta}^2}{2} + \\ &+ \frac{J_1 \dot{\theta}_1^2}{2} + \frac{J_2 \dot{\theta}_2^2}{2}, \end{aligned} \quad (7)$$

where $R \equiv R(t)$ is the relative motion coordinate; $\dot{R}(t)$ is the corresponding velocity; α_T is the orientation angle between beam direction and axial symmetry axis of the target (Cf isotope); L_0 ($L_0 = \ell_0 \hbar$) and E_{rot} are defined by initial conditions; J_R and $\dot{\theta}$, J_1 and $\dot{\theta}_1$, J_2 and $\dot{\theta}_2$ are moment of inertia and angular velocities of the DNS and its fragments, respectively; γ_R and γ_{θ} are the friction coefficients for the relative motion along R and the tangential motion when two nuclei roll on each other's surfaces, respectively; C_{β_i} and γ_{β_i} , and D_{β_i} are stiffness, damping and mass coefficients for the surface vibrations of ^{48}Ca , respectively; $V(R, \alpha_T)$ is the nucleus-nucleus potential calculated by the double folding procedure [18, 19]. Friction coefficients γ_R and γ_{θ} depend on the shell structure of interacting nuclei (see Ref. [20] and Appendix A of Ref. [21]) and orientation angles of their axial symmetry axes (if they are deformed). Our

calculations showed that ratio between them does not change so much during capture trajectory of collision: $\gamma_\theta/\gamma_R = 3 \cdot 10^{-3} \div 4 \cdot 10^{-3}$. The values of surface vibration coefficients for the quadrupole multipolarity are given in Ref. [22]. The values of damping coefficient γ_{β_i} for the surface vibration are calculated by the expression presented in Ref. [17]. The deformation parameters in the ground state of $^{249-252}\text{Cf}$ were obtained from Ref. [23].

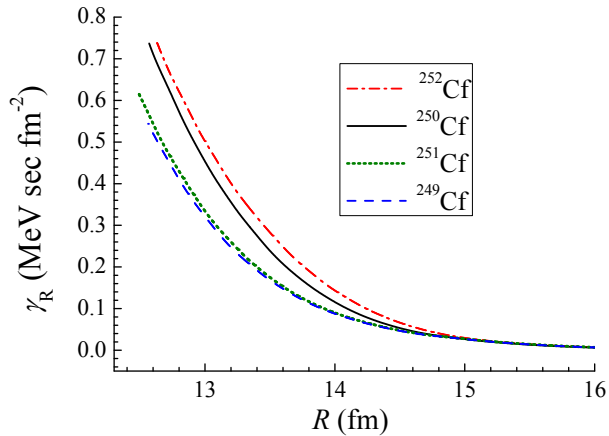


FIG. 2. (Color online) Comparison of the radial friction coefficient γ_R for the $^{48}\text{Ca}+^{249-252}\text{Cf}$ reactions. The presented results were obtained for the orientation angle $\alpha = 30^\circ$ of the axial symmetry axis of Cf isotopes.

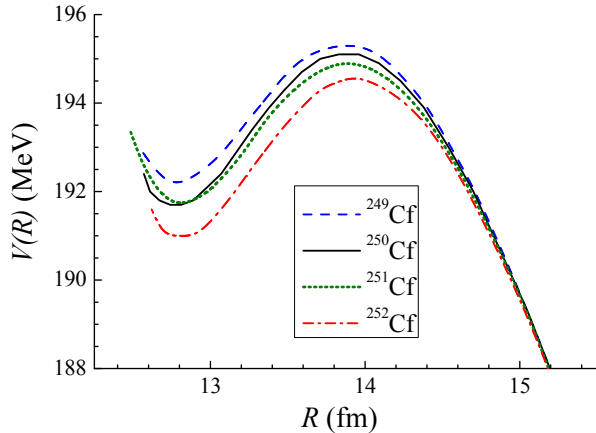


FIG. 3. (Color online) Comparison of the nucleus-nucleus potential $V(R)$ for the $^{48}\text{Ca}+^{249-252}\text{Cf}$ reactions. The presented results were obtained for the orientation angle $\alpha = 30^\circ$ of the axial symmetry axis of Cf isotopes.

The results of calculation are partial capture cross sections corresponding to the angular momentum distribution of the DNS formed after full momentum transfer. The probability of capture event is sensitive to the nucleus-nucleus potential and friction coefficient which depend on the single-particle states of protons and neutrons in the interacting nuclei [20]. The last quantities

are sensitive to the mass number of the given isotope. In Fig. 1 we compare the capture cross sections calculated for the $^{48}\text{Ca}+^{249-252}\text{Cf}$ reactions which can lead to formation of compound nuclei being appeared as isotopes of the 118 superheavy element with mass numbers $A = 297, 298, 299,$ and 300 .

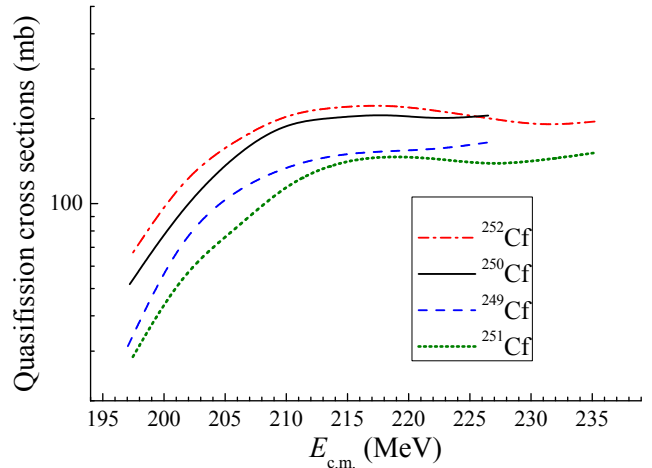


FIG. 4. (Color online) Comparison of the quasifission cross sections for the $^{48}\text{Ca}+^{249-252}\text{Cf}$ reactions.

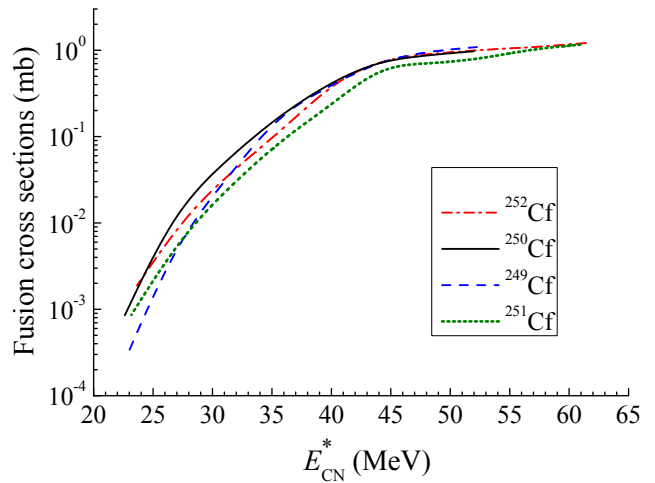


FIG. 5. (Color online) Comparison of the fusion cross sections for the $^{48}\text{Ca}+^{249-252}\text{Cf}$ reactions.

The study of the effect of mass number A on the capture process is reduced to analyze the dependence of the friction coefficient and nucleus-nucleus potential on A . In Fig. 2 we compare the friction coefficients which were calculated for the $^{48}\text{Ca}+^{249-252}\text{Cf}$ reactions and for the orientation angle $\alpha_T = 30^\circ$ of the axial symmetry axis of Cf isotopes. As one can see the friction coefficients which were obtained for the $^{48}\text{Ca}+^{250,252}\text{Cf}$ reactions with even isotopes of Cf are appreciably higher than

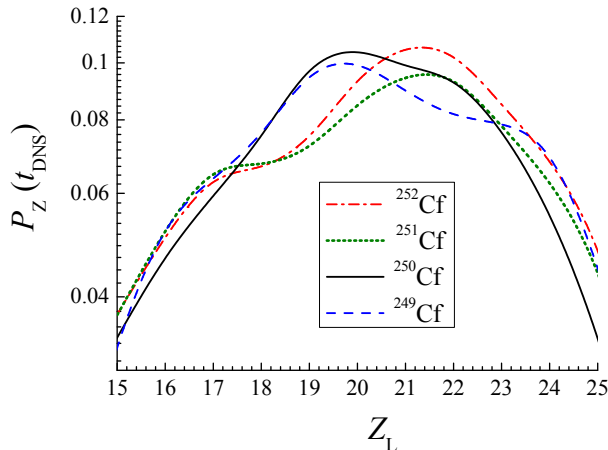


FIG. 6. (Color online) Comparison of the behaviour of the charge distributions between constituents of dinuclear system formed in the $^{48}\text{Ca}+^{249-252}\text{Cf}$ reactions. The results are obtained for the evolution of dinuclear system during $t_{\text{DNS}} = 3 \cdot 10^{-21}$ s.

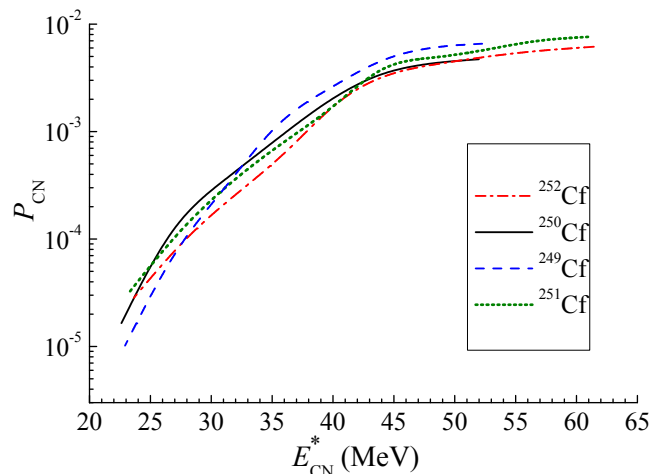


FIG. 7. (Color online) Comparison of the P_{CN} fusion probability for the $^{48}\text{Ca}+^{249-252}\text{Cf}$ reactions.

the ones calculated for the $^{48}\text{Ca}+^{249,251}\text{Cf}$ reactions with its odd isotopes. In addition, Fig. 3 shows the comparison of the depth of the potential wells which are responsible for the capture of nuclei; from this figure appears that in reactions with even isotopes of Cf the potential wells are deeper than the ones obtained for the reactions with odd isotopes of Cf. The shell effects are included into a term $\delta V(R)$ of the nucleus-nucleus potential

$$V(R) = V_{\text{Coul}}(R) + V_{\text{nuc}}(R) + V_{\text{rot}}(R) + \delta V(R), \quad (8)$$

where $V_{\text{Coul}}(R)$ is the Coulomb interaction potential which is calculated by Wong's formula [24]; V_{nuc} is nuclear part which is found by double folding procedure with the effective nucleon-nucleon forces [25]; V_{rot} is DNS rotational energy. The nature of $\delta V(R)$ term and friction

coefficient γ_R are connected with nucleon exchange between nuclei [21]:

$$\delta V(R(t)) = \sum_{i,k} \left| \frac{\partial V_{ik}(R)}{\partial R(t)} \right|^2 B_{ikj}^{(0)}(R(t)), \quad (9)$$

$$\gamma_R = \sum_{i,k} \left| \frac{\partial V_{ik}(R)}{\partial R(t)} \right|^2 B_{ikj}^{(1)}(R(t)), \quad (10)$$

where

$$B_{i,k}^{(n)}(R(t)) = \frac{2}{\hbar} \int_{t_0}^t dt (t-t_0)^n \exp[(t-t_0)/\tau_{ik}] \times \sin[\omega_{ik}(R(t))(t-t_0)](n_i - n_k), \quad (11)$$

$$\text{with } \hbar\omega_{ik} = \epsilon_i + \Lambda_{ii} - \epsilon_k - \Lambda_{kk}, \quad (12)$$

containing the dependence on the single-particle occupation numbers n_i and energies ϵ_k of nucleons in the interacting nuclei (i and k states belong to projectile and target nuclei, respectively); Λ_{ii} and Λ_{kk} are diagonal elements of the matrix elements V_{ik} of the DNS meanfield for nucleons; n_i is the diagonal matrix element of the density matrix which is calculated according to the model presented elsewhere [20, 26];

$$\tau_{ik} = \frac{\tau_i \cdot \tau_k}{\tau_i + \tau_k}, \quad (13)$$

τ_i (τ_k) is the lifetime of the quasiparticle excitations in the single-particle state i (k) of each reacting nucleus. It determines the damping of single-particle excitation. τ_i (τ_k) is calculated using the results of the quantum liquid theory [27] and the effective nucleon-nucleon forces from [25] as in Ref. [20].

From this analysis we can conclude that the difference between capture cross sections presented in Fig. 1 is caused by difference in occupation single-particle states in different isotopes of Cf. This difference quantitatively appears in the friction coefficient of the radial motion and nucleus-nucleus interaction.

In calculation of the fusion cross section we use the potential energy surface of dinuclear system which includes the binding energies of the interacting nuclei (B_1 and B_2) and compound nucleus (B_{CN}): $U_{\text{dr}} = B_1 + B_2 - B_{\text{CN}} + V_{\text{nuc-nuc}}$ where $V_{\text{nuc-nuc}}$ is the nucleus-nucleus interacting potential. Therefore, the landscape of the potential energy surface determines competition between complete fusion and quasifission during evolution of DNS [18, 19, 21]. As discussed in these papers, during evolution to compound nucleus, the dinuclear system must overcome the intrinsic fusion barrier B_{fus}^* which is determined by its mass and charge asymmetry, as well as shell structure and orientation angles of symmetry axes of its constituents. Therefore, the fusion probability of the dinuclear system into compound nucleus P_{CN} at the given excitation energy E_{DNS}^* is calculated as a sum of fusion

probabilities from different configuration with different charge asymmetries:

$$P_{\text{CN}}(E_{\text{DNS}}^*, \ell, \alpha_T) = \sum_{Z=Z_{\text{sym}}}^{Z=Z_{\text{max}}} Y_Z(E_{\text{DNS}}^{*(Z)}, \ell, \alpha_T) \times P_{\text{CN}}^{(Z)}(E_{\text{DNS}}^*(Z), \ell, \alpha_T) \quad (14)$$

where $E_{\text{DNS}}^* = E_{\text{c.m.}}V(Z, R_m, \ell, \alpha_T) + \Delta Q_{\text{gg}}(Z)$ is the excitation energy of DNS for a given value of its charge-asymmetry configuration $(Z, Z_{\text{tot}} - Z)$ and $Z_{\text{tot}} = Z_1 + Z_2$; $E_{\text{c.m.}}$ is the collision energy in the center-of-mass system; $V(Z, R_m, \ell; \alpha_T)$ and R_m are the minimum value of the nucleus-nucleus potential well and its position on the relative distance between centers of nuclei; $\Delta Q_{\text{gg}}(Z)$ is the change of $Q_{\text{gg}}(Z)$ -value by changing the DNS charge asymmetry from the initial value $Z = Z_1$; $P_Z(E_{\text{DNS}}^{*(Z)})$ and $Y_Z(E_{\text{DNS}}^{*(Z)})$ are the probabilities of population of the configuration $(Z, Z_{\text{tot}} - Z)$ at $E_{\text{DNS}}^{*(Z)}$ and decay from this configuration, respectively. $Z_{\text{sym}} = (Z_1 + Z_2)/2$ and Z_{max} corresponds to the point where the driving potential reaches its maximum value ($B_{\text{fus}}(Z_{\text{max}}) = 0$) (see Refs. [18, 19, 21]).

The theoretical results presented in Fig. 4 show that the behaviours of the quasifission excitation functions for the reactions under discussion are similar to the corresponding capture excitation functions shown in Fig. 1, while the difference fusion excitation functions (the formalism is shortly presented in Appendix A and references therein) calculated for these reactions is not so much as for capture excitation function: the values of the fusion excitation functions are closer (see Fig. 5). The reason for which the advance in capture of the $^{48}\text{Ca}+^{250,252}\text{Cf}$ reactions with even isotopes of Cf in comparison with the $^{48}\text{Ca}+^{249,251}\text{Cf}$ reactions has been lost is explained by the opposite behaviour of the charge distribution between constituents of DNS which is formed in the initial stage of the reactions. As one can see in Fig. 6 the maximum of the charge distribution in DNS formed in the reactions with isotopes of Cf with larger ($A=251$ and 252) mass numbers moves to the charge symmetric direction while the charge distribution of ones formed in the reactions with isotopes of Cf with smaller mass numbers ($A=249$ and 250) moves to charge asymmetric direction. It is known from theoretical models based on the DNS concept [28] and our calculations that hindrance to complete fusion increases for the more charge symmetric configurations because in this case intrinsic fusion barrier increases and quasifission barrier decreases making system less stable against decay into two fissionlike fragments (we call them quasifission fragments) [8]. Therefore, although the capture excitation function of the $^{48}\text{Ca}+^{249}\text{Cf}$ reaction was lower but its fusion excitation function grows more fastly than the ones of the other reactions by increasing the beam energy and becomes even higher (Fig. 5).

The fusion probability P_{CN} (see Fig. 7) determines fusion cross section at the given capture cross section and, therefore, its behaviour is similar of the behaviour of the

fusion excitation function presented in Fig. 5. The close values of the calculated fusion cross sections of all reactions mean that the difference in the evaporation residue cross sections for the $^{48}\text{Ca}+^{249-252}\text{Cf}$ reactions may appear in dependence of the survival probability of compound nucleus and excited intermediate nuclei along the de-excitation cascade of CN on its mass number A_{CN} .

III. EVAPORATION RESIDUE CROSS SECTION AND DISCUSSION

The excitation function of the individual evaporation residues (ER) along the de-excitation cascade of compound nuclei formed in the investigated $^{48}\text{Ca}+^{249,250,251,252}\text{Cf}$ reactions are calculated by formula (see Refs. [29, 30])

$$\sigma_{\text{ER}}^{(x)}(E_x^*) = \sum_{\ell=0}^{\ell_d} (2\ell+1) \sigma^{(x-1)}(E_x^*, \ell) W_{\text{sur}}^{(x-1)}(E_x^*, \ell), \quad (15)$$

where $\sigma^{(x-1)}(E_x^*, \ell)$ is the partial formation cross-section of the excited intermediate nucleus of the $(x-1)$ th step and $W_{\text{sur}}^{(x-1)}(E_x^*, \ell)$ is the survival probability of the $(x-1)$ th intermediate nucleus against fission along the de-excitation cascade of CN. It is clear that $\sigma^{(0)}(E_x^*, \ell) = \sigma_{\text{fus}}(E_x^*, \ell)$. The maximum value ℓ_d of partial waves contributing to capture events is found by solving the equations of motion (1)-(7) for the given initial values of the energy $E_{\text{c.m.}}$ and orbital angular momentum ℓ_0 of collision, at each value orientation angle α_T of the axial symmetry of the deformed target nucleus (in details see Ref. [21]). We should stress that the real number of partial waves contributing to the ER formation is much smaller than ℓ_d because $W_{\text{sur}}^{(x-1)}(E_x^*, \ell)$ depends on the fission barrier being a sum of the parameterized macroscopic fission barrier $B_{\text{fis}}^m(\ell)$ depending on the angular momentum J and the microscopic (shell) correction δW

$$B_{\text{fis}}(\ell, T) = c B_{\text{fis}}^m(\ell) - h(T) q(\ell) \delta W. \quad (16)$$

In our calculations, superheavy isotopes of element $Z = 118$ have not macroscopic barrier, $B_{\text{fis}}^m(\ell) = 0$ and we took into account damping of the shell correction by increasing the excitation energy E_x^* and ℓ angular momentum of fissioning nucleus by the functions $h(T)$ and $q(\ell)$, respectively. These functions are

$$h(T) = \{1 + \exp[(T - T_0)/d]\}^{-1} \quad (17)$$

and

$$q(\ell) = \{1 + \exp[(\ell - \ell_{1/2})/\Delta\ell]\}^{-1}, \quad (18)$$

where, in Eq. (17), $d = 0.3$ MeV is the rate of washing out the shell corrections with the temperature, and $T_0 = 1.16$ MeV is the value at which the damping factor $h(T)$ is reduced by 1/2; analogously, in Eq. (18),

$\Delta\ell = 3\hbar$ is the rate of washing out the shell corrections with the angular momentum, and $\ell_{1/2} = 20\hbar$ is the value at which the damping factor $q(\ell)$ is reduced by 1/2. This procedure allows the shell corrections to become dynamical quantities, also. Therefore, if the capture of ^{48}Ca by an isotope of Cf takes place up to values $\ell_d = 105$ the fission barrier disappears at $\ell > 40$ due to damping the shell correction by $q(\ell)$.

The partial cross section of complete fusion is calculated by formula (see Refs. [29, 30])

$$\sigma_{\text{fus}}(E_{\text{c.m.}}, \ell; \beta_P, \alpha_T) = \sigma_{\text{cap}}(E_{\text{c.m.}}, \ell; \beta_P, \alpha_T) \times P_{\text{CN}}(E_{\text{c.m.}}, \ell; \beta_P, \alpha_T), \quad (19)$$

In Fig. 8 we report the ER cross sections for the $^{48}\text{Ca}+^{249}\text{Cf}$ reaction after emission of 2, 3, 4, and 5 neutrons from the $^{297}\text{118}$ CN as a function of the E_{CN}^* excitation energy. The calculated ER cross sections were obtained by using the mass and fission barrier values given in Refs. [31, 32] of the Warsaw group.

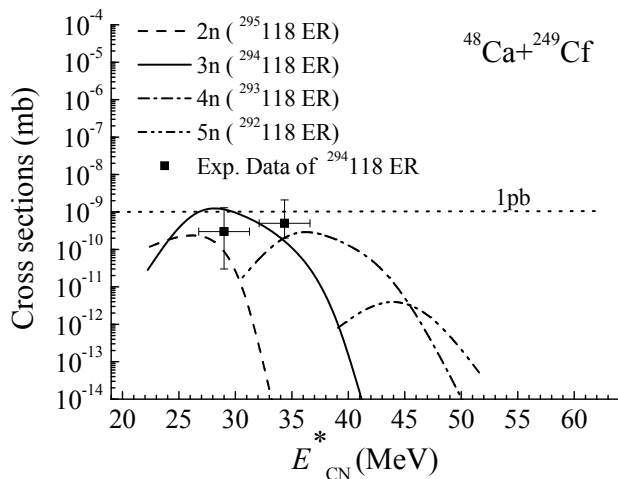


FIG. 8. Individual evaporation residue excitation functions after emission of 2 (dashed line), 3 (full line), 4 (dash-dotted line), and 5 (dash-double dotted line) neutrons from the $^{297}\text{118}$ CN in the $^{48}\text{Ca}+^{249}\text{Cf}$ reaction, by using in calculation the masses and fission barrier values of Refs. [31, 32]. The experimental data (full squares) of the $^{294}\text{118}$ ER formation cross section obtained from Ref.[16].

Since the fission barrier component of the macroscopic rotating liquid drop model is zero for the formed superheavy nuclei, the component caused by the shell effects (microscopic model) is damped by a function depending on the nuclear temperature and angular momentum of CN (see Ref. [19]). In this figure we present the data obtained in the $^{48}\text{Ca}+^{249}\text{Cf}$ experiment reported in Ref. [16] regarding the synthesis of the $^{294}\text{118}$ superheavy nucleus obtained after 3 neutron emission from the $^{297}\text{118}$ CN, at two projectile energies corresponding to excitation energies of $E^* = 29.2$ and 34.4 MeV of the compound nucleus. As Fig. 8, shows the maximum values of

cross sections connected with the 2n, 3n, and 4n emission channels are included in the 0.3–1.2 pb range. It is possible, in principle, to detect the $^{295}\text{118}$, $^{294}\text{118}$, and $^{293}\text{118}$ evaporation residue nuclei which formed after emission of 2, 3, and 4 neutrons, respectively, from the $^{297}\text{118}$ CN, at convenient ^{48}Ca beam energies in the 241 – 253 MeV interval. In this figure, the result of the $^{294}\text{118}$ evaporation excitation function (3n channel) is in fairly good agreement with the experimental data of Ref. [16]. In fact, the calculated values of the ER cross sections at $E_{\text{CN}}^* = 29.2$ and 34.4 MeV are close to the experimental data barely within the error bars. For this reason we decided to continue analysis and interpret the origination of difference between our results and observed experimental data (see in forward Fig. 14).

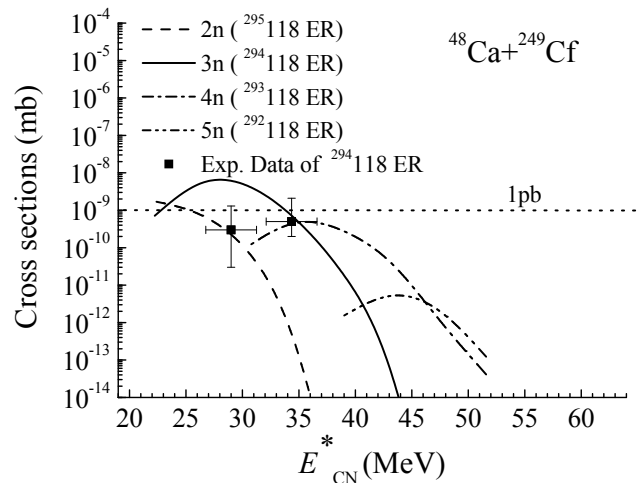


FIG. 9. As Fig. 8, but by using in calculation the masses of Ref. [23] and fission barriers of Ref. [33].

In Fig. 9 we report the analogous results as shown in Fig. 8, obtained for the same $^{48}\text{Ca}+^{249}\text{Cf}$ reaction leading to the $^{297}\text{118}$ CN, but by using in the calculation the masses of Ref. [23] and the fission barriers of Ref. [33] given by Möller *et. al.* As the figure shows, the excitation function of the 3n evaporation channel is in good agreement with the second experimental point only, but in general the excitation functions of evaporation residue nuclei by this way are higher than the results obtained by using the masses [31] and fission barriers [32] of the Warsaw group. The comparison of the results calculated by the both set of theoretical masses and barriers with the experimental data from Ref. [16] is shown in Fig. 10. All results obtained by using the two different masses and barriers data were performed with the same set of other parameters above-described in this paper.

In the following Figs. 11, 12 and 13 we compared the ER excitation functions obtained in this work by using the masses and barriers of Refs. [31, 32] (thick lines) and Refs. [23, 33] (thin lines) for the other $^{48}\text{Ca}+^{250,251,252}\text{Cf}$ investigated reactions leading to the $^{298}\text{118}$, $^{299}\text{118}$, and

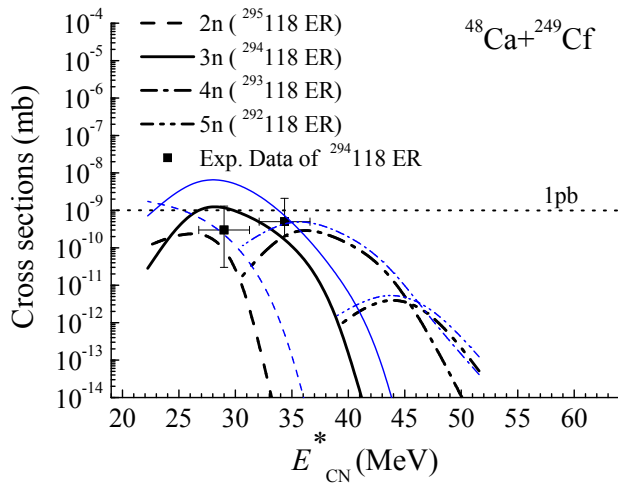


FIG. 10. (Color online) Comparison of results reported in Figs. 8 and 9. Thick lines are obtained by using the values of Refs. [31, 32], thin lines by using the values of Refs. [23, 33].

$^{300}118$ compound nuclei, respectively. The maximum values of the ER excitation functions for the 3n emission channel reach or overestimate 10 pb when the mass and fission barrier values of Refs. [23, 33] are used, moreover, these values are larger than experimental data of Ref. [16] and more higher than the corresponding values which have been found when the masses and barriers of Refs. [31, 32] are used. Therefore, in the following analysis we choose to refer to the excitation functions (thick lines) obtained by using masses and barriers of Refs. [31, 32] because the results appear more closer to the experimental data.

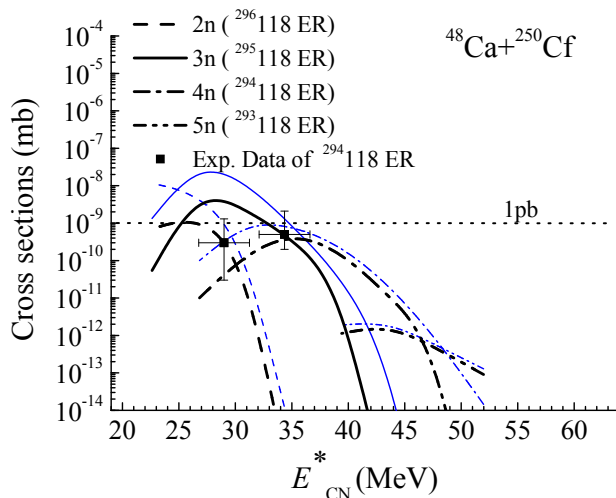


FIG. 11. (Color online) As Fig. 10, but for the $^{48}\text{Ca}+^{250}\text{Cf}$ reaction.

As one can see in Fig. 11, the cross section calculated for the $^{294}118$ evaporation residue nucleus, which is ob-

tained after emission of 4 neutrons from the $^{298}118$ CN being a product of the $^{48}\text{Ca}+^{250}\text{Cf}$ reaction, is also in good agreement with the data of the $^{294}118$ evaporation residue synthesized in the $^{48}\text{Ca}+^{249}\text{Cf}$ experiment after 3 neutron emission from $^{297}118$ CN.

In the experimental identification of the ER nucleus by the α -decay chain assures only the $^{294}118$ formation but the predecessor de-excitation cascade-3 neutrons emission from the $^{297}118$ CN or 4 neutrons emission from the $^{298}118$ CN can not be distinguished. The problem is that the presence of the ^{250}Cf isotope in the used target in addition with the ^{249}Cf isotope is inevitable and therefore it is necessary to take into account the $^{294}118$ contributions caused by the both $^{48}\text{Ca}+^{249}\text{Cf}$ and $^{48}\text{Ca}+^{250}\text{Cf}$ reactions.

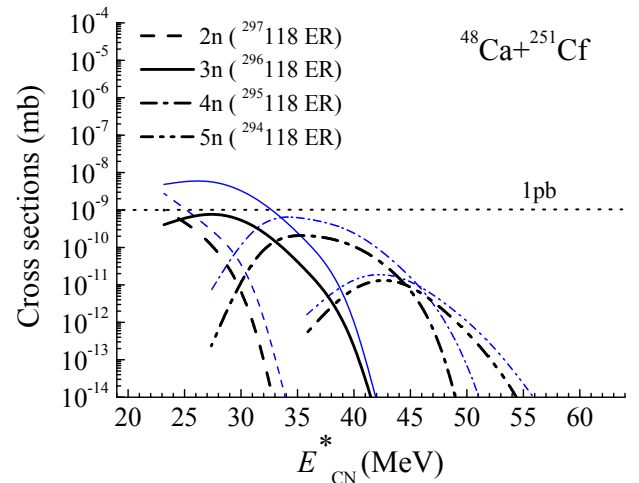


FIG. 12. (Color online) As Fig. 10, but for the $^{48}\text{Ca}+^{251}\text{Cf}$ reaction.

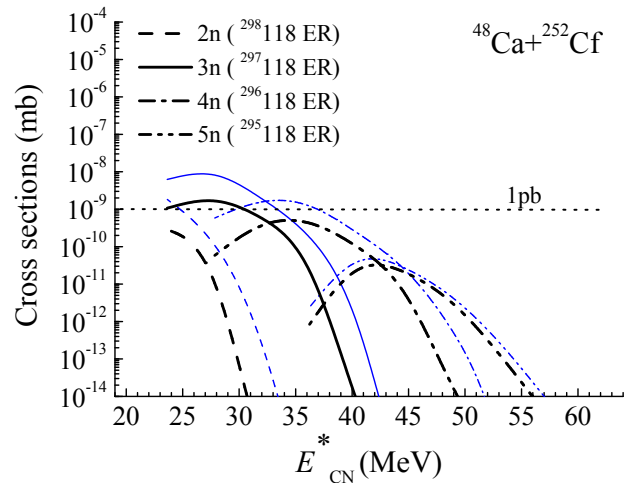


FIG. 13. (Color online) As Fig. 10, but for the $^{48}\text{Ca}+^{252}\text{Cf}$ reaction.

In Fig. 14 we report the excitation functions of the 3n evaporation channel in the reaction with the ^{249}Cf

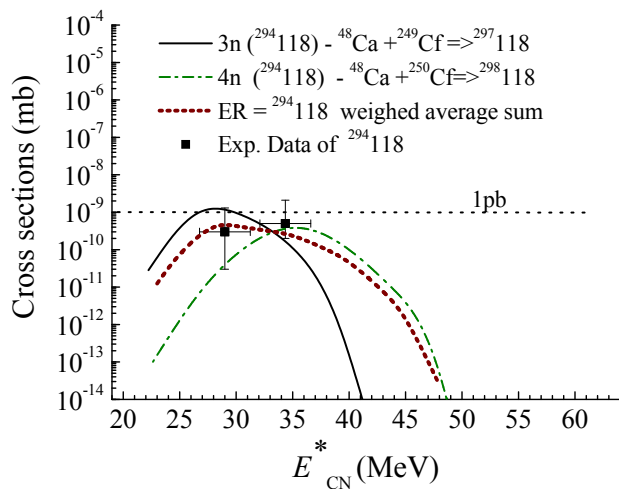


FIG. 14. (Color online) Contributions of the $^{294}\text{118}$ evaporation residue nucleus synthesized by the $^{48}\text{Ca}+^{249}\text{Cf}$ (full line) and $^{48}\text{Ca}+^{250}\text{Cf}$ (dash-dotted line) reactions. The dotted line represents the weighed average sum of the two mentioned contributions.

isotope and 4n evaporation channel in the reaction with ^{250}Cf isotope, as well as the experimental data from Ref. [16]. In this figure we add the weighed two excitation functions of the same $^{294}\text{118}$ evaporation residue nucleus reached by both $^{48}\text{Ca}+^{249,250}\text{Cf}$ reactions after 3 and 4 neutron emission, respectively (see Figs. 8 and 11), represented by the dotted line in Fig. 14. As one can see, this averaged excitation function of the $^{294}\text{118}$ formation is in complete agreement with the data of Ref. [16].

As regards the possibility to detect also the formation of $^{295}\text{118}$ ER nucleus obtained after 3n emission from the $^{298}\text{118}$ CN in the $^{48}\text{Ca}+^{250}\text{Cf}$ reaction (see Fig. 11), we observe that this ER nucleus reaches the maximum yield of about 4 pb at $E_{\text{CN}}^* = 28$ MeV of the $^{298}\text{118}$ CN. Moreover, at $E_{\text{CN}}^* = 35$ MeV the $^{295}\text{118}$ ER formation reaches the appreciable value of 0.6 pb obtained as sum of the contribution due to the 3 neutron emission from the $^{298}\text{118}$ CN in the $^{48}\text{Ca}+^{250}\text{Cf}$ reaction (see Fig. 11) and also the contribution due to the $^{295}\text{118}$ ER formation after 4 neutron emission from $^{299}\text{118}$ CN in the $^{48}\text{Ca}+^{251}\text{Cf}$ reaction (see Fig. 12). Moreover, as one can see in Fig. 13 the population of the 3n-channel (corresponding to the $^{297}\text{118}$ ER formation) should reach about 2 pb at the E_{CN}^* excitation energy of 27-28 MeV of the $^{300}\text{118}$ CN while the population of the 4n-channel (leading to the $^{296}\text{118}$ ER) is near 0.5 pb at the E_{CN}^* excitation energy of about 35 MeV of the $^{300}\text{118}$ CN. Therefore, the $^{48}\text{Ca}+^{252}\text{Cf}$ reaction also appears as an useful and accessible reaction in order to obtain the $^{297}\text{118}$ and $^{296}\text{118}$ ER nuclei after 3n and 4n emission from the $^{300}\text{118}$ CN, respectively.

One can see in Figs. 10-13 that the highest yield of ER nuclei formation in the $E_{\text{CN}}^* = 25 - 40$ MeV excitation energy interval is obtained for the 3n-channel of the

four investigated reaction, but the 2n- and 4n-channel are also populated by an appreciable mode. Of course, the experimental data observed in the $^{48}\text{Ca}+^{249}\text{Cf}$ reaction [16] corresponding to the formation of the $^{294}\text{118}$ ER at $E_{\text{CN}}^* = 29.2$ and 34.4 MeV may be meaningfully considered as contributions of the 3n-channel of the $^{48}\text{Ca}+^{249}\text{Cf}$ reaction and the 4n-channel of the $^{48}\text{Ca}+^{250}\text{Cf}$ reaction. If we assume a hypothesis that the target contains also the ^{251}Cf and ^{252}Cf isotopes, we can verify that the contributions of the $^{294}\text{118}$ ER nucleus formed in the $^{48}\text{Ca}+^{251,252}\text{Cf}$ reactions are very small (lower than 10^{-9} and 10^{-6} pb, respectively) in the above-mentioned 29.2 - 34.4 MeV excitation energy interval of the corresponding CN, because the $^{294}\text{118}$ ER nucleus should be reached after 5n emission from the $^{299}\text{118}$ CN, and 6n emission from the $^{300}\text{118}$ CN. Therefore, in the excitation energy range 29.2 - 34.4 MeV, only the events of the 4n emission from the $^{298}\text{118}$ CN formed in the $^{48}\text{Ca}+^{250}\text{Cf}$ reaction can contribute to the population of the $^{294}\text{118}$ ER nucleus (see thick dashed line in Fig. 11) in addition to the contribution of the 3n emission from the $^{297}\text{118}$ CN formed in the $^{48}\text{Ca}+^{249}\text{Cf}$ reaction (see full line in Fig. 8).

Moreover, as Figs. 10, 11, 12, and 13 show, the evaporation residue yields for the 2n, 3n, 4n, and 5n channels for the reactions with even-even $^{250,252}\text{Cf}$ targets are higher than for the ones with even-odd $^{249,251}\text{Cf}$ targets. The ER excitation functions calculated by using the masses and barriers of Ref. [23] are higher than the ones obtained by using the values of Refs. [31, 32]. By the comparison of the excitation functions of ER in reactions leading to the $^{297-300}\text{118}$ CN's, we can affirm that the use of masses and barriers of Refs. [31, 32] in calculation of the evaporation residue nuclei leads to the results which are close to the experimental data while the values obtained from Ref. [23, 33] lead to overestimation them. Moreover, one can observe from results from Figs. 10-13 that the cross sections determined for the ER nuclei obtained after 2n, 3n, and 4n emission from the $^{297-300}\text{118}$ CN's are included in the about 0.2 - 4 pb range in the $E_{\text{CN}}^* = 25 - 40$ MeV excitation energy region of the corresponding CN which are formed in the $^{48}\text{Ca}+^{249-252}\text{Cf}$ reactions. Therefore, the events and related cross section of the $^{293-298}\text{118}$ ER nuclei yields in the $^{48}\text{Ca}+^{249-252}\text{Cf}$ reactions can be observed and measured. The $^{293}\text{118}$ and $^{298}\text{118}$ ER nuclei can be only observed in the $^{48}\text{Ca}+^{249}\text{Cf}$ and $^{48}\text{Ca}+^{252}\text{Cf}$, respectively, while the other pairs $^{294,295}\text{118}$, $^{295,296}\text{118}$, and $^{296,297}\text{118}$ ER nuclei can be observed in the $^{48}\text{Ca}+^{249,250}\text{Cf}$, $^{48}\text{Ca}+^{250,251}\text{Cf}$, and $^{48}\text{Ca}+^{251,252}\text{Cf}$ reactions, respectively, with respect to the presence of contiguous Cf isotopes in target. In this case, instead to work with a target enriched with one of Cf isotope only, it is convenient to have one target constituted of two or more isotopes of Cf (as for example $^{249,252}\text{Cf}$) because at various ^{48}Ca beam energies the contiguous evaporation residue yields produced by xn-channels of the two reactions can be explored. The rate of ER contributions depends on the ^{48}Ca beam energy

(and then with the E_{CN}^* energy) and also on the peculiarities of the ER formation channels. The presence of various contiguous isotopes in target gives the possibility to observe different ER nuclei in the same experiment and to compare the rate of various ER yields. In such a case the preparation of the target is less expansive for cost and time, and the set of experimental data is more rich in yields and variety of registered ER nuclei.

In addition to our previous analysis and discussion, it is useful to compare the results of the excitation functions presented in Fig. 12 of this paper for the $^{48}\text{Ca}+^{251}\text{Cf}$ reaction (when the values of masses and fission barriers of Refs. [31, 32] are used) with the corresponding results given in Fig. 3 (b) of Ref. [34] for the same reaction. Apart from the fact that the excitation functions of the main 3n- and 4n- channel of Ref. [34] are about 2 and 3 times, respectively, higher than our corresponding values reported in Fig. 12. It seems to be not realistic that the 2n- and 3n- excitation functions are peaked at 35 and 36 MeV of excitation energy, respectively. In the formation of evaporation residue with about 0.1 pb cross section 2 emitted neutrons take away 42 MeV from the $^{299}118$ CN against about 13 MeV requested for the neutron binding energy of 2 neutrons. It means that each neutron should move with a kinetic energy of about 14 – 15 MeV while in average the neutron kinetic energy is close to the CN temperature in this case which is about 0.9 MeV. Analogously for the 3n channel where at 0.1 pb of ER cross section the 3 emitted neutrons take away 48 MeV from the compound nucleus against about 19.5 MeV requested for the neutron binding energy of 3 neutrons. Also in this case each neutron moves with a kinetic energy of about 10 MeV in comparison with the nuclear temperature of the compound nucleus that is about 1 MeV. That is an unrealistic result. In fact, in our evaporation residue excitation functions reported in Figs. 8-14, the results always lead to an average neutron kinetic energy of about 0.9 - 1 MeV.

In conclusion of the present discussion, we can affirm that our complete model is able to describe the evolution of dinuclear system during reaction up to the CN formation and CN's de-excitation cascade. This model leads to reliable results of individual excitation functions of evaporation residue nuclei as a function of energy and orbital angular momentum for each projectile-target combination (see Refs. [15, 35, 36]).

IV. CONCLUSIONS

We investigated the formation of the heaviest evaporation residue nuclei from the $^{297-300}118$ CN which are formed in reactions induced by collision of the ^{48}Ca projectiles with the heaviest accessible actinide targets $^{249-252}\text{Cf}$. If in future it will be possible to prepare targets of ^{254}Es and ^{257}Fm , then the $^{302}119$ and $^{305}120$ CN's may be formed, but these targets are in every way the extreme limit of possibility of synthesizing SHE's by using

the ^{48}Ca beam because other heavier Es and Fm nuclei as well as other heavier actinide nuclei are radioactive with shorter lifetimes. Therefore, it is impossible to prepare useful targets with the aim to synthesize superheavy elements heavier than $^{302}119$ and $^{305}120$ by ^{48}Ca induced reactions.

By analyzing the 2, 3, 4, and 5 neutron emission channels along the de-excitation cascade of compound nuclei formed in the $^{48}\text{Ca}+^{249-252}\text{Cf}$ reactions we studied the possibilities of synthesizing the $^{292-298}118$ ER nuclei. In addition, by considering the experimental conditions nowadays available in Laboratories, the more convenient and accessible reaction channels of observing evaporation residue nuclei are the 3 and 4 neutron emission channels in the $^{48}\text{Ca}+^{249-252}\text{Cf}$ reactions at beam energies corresponding to the $E^* = 25 - 40$ MeV excitation energy range of compound nuclei.

Moreover, we found higher capture cross sections for the $^{48}\text{Ca}+^{250,252}\text{Cf}$ reactions in comparison with the ones of the $^{48}\text{Ca}+^{249,251}\text{Cf}$ reactions. We discussed the influence of the entrance channel dynamics on the capture, quasifission, and fusion cross sections by considering the mass asymmetry parameter, shell effects of reactants, dynamical deformation of nuclei in the DNS formation, interaction angle between the axial symmetry axes at collision of projectile and target nuclei. We also considered the effects of masses and fission barriers on the evaporation residue nuclei when the values of Refs. [31, 32] or the ones of Ref. [23, 33] are used.

By comparing the results of our analysis regarding the study of the $^{48}\text{Ca}+^{249,250}\text{Cf}$ reactions with the data obtained in the experiment of Ref. [16] regarding the observation of the $^{294}118$ evaporation residue nucleus, we conclude that the better description of the experimental results is that the observed $^{294}118$ synthesis events [16] registered at two different beam energies are contributed by the 3n-channel in the $^{48}\text{Ca}+^{249}\text{Cf}$ reaction and 4n-channel in the $^{48}\text{Ca}+^{250}\text{Cf}$ reaction, due to the inevitable presence of the ^{250}Cf isotope in the ^{249}Cf enriched target. Moreover, the comparison of results obtained for the ER nuclei in the investigation of the $^{48}\text{Ca}+^{252}\text{Cf}$ reaction suggest to use one target only constituted of all the Cf isotopes of more long lifetimes. It is more convenient the procedure for its preparation, and in one experiment only it is possible to observe and study a wide set of ER nuclei formed by 2n, 3n, 4n, and 5n emission channels, only changing the ^{48}Ca beam energy in the about $E_{\text{lab}} = 235 - 260$ MeV range.

ACKNOWLEDGMENTS

A.K. Nasirov is grateful to the Istituto Nazionale di Fisica Nucleare and Department of Physics of the University of Messina for the support received in the collaboration between the Dubna and Messina groups, and he thanks the Russian Foundation for Basic Research for the financial support in the performance of this work.

A. Sobiczewski would like to thank Yu. Oganessian, J. Roberto, and V. Utyonkov for useful discussions about the questions connected with the possible use of the californium target, which should be a mixture of isotopes

, in the synthesis of the 118 element. A. S. acknowledges a support by the Polish National Centre of Science (within the research project No. N N 202 204938) and the Polish-JINR (Dubna) Cooperation Programme.

-
- [1] Yu. Ts. Oganessian *et al.*, Phys. Rev. C **72**, 034611 (2005).
- [2] Yu. Ts. Oganessian *et al.*, Phys. Rev. C **69**, 054607 (2004).
- [3] Yu. Ts. Oganessian *et al.*, Phys. Rev. Lett. **104**, 142502 (2010).
- [4] Yu. Ts. Oganessian *et al.*, Phys. Rev. C **79**, 024603 (2009).
- [5] S. Hofmann *et al.*, GSI Scientific Report No. PHN-NUSTARSHE-01. 205 (2011).
- [6] Ch.E. Düllmann *et al.*, GSI Scientific Report No. PHN-NUSTAR-SHE-02, 206 (2011).
- [7] A.K. Nasirov, G. Giardina, G. Giardina, A. Sobiczewski, A.I. Muminov, Phys.Rev. C **84**, 044612 (2011).
- [8] A. K. Nasirov, G. Giardina, G. Mandaglio, and M. Manganaro, F. Hanappe, S. Heinz and S. Hofmann, A. I. Muminov, W. Scheid, Phys.Rev. C **79**, 024606 (2009).
- [9] Valery Zagrebaev and Walter Greiner, Phys. Rev. C **78**, 034610 (2008).
- [10] Z. H. Liu and Jing-Dong Bao, Phys. Rev. C **80**, 054608 (2009).
- [11] G.G. Adamian N.V. Antonenko, and W. Scheid, Eur. Phys. J. A **41**, 235 (2009).
- [12] K. Siwek-Wilczyńska, T. Cap, J. Wilczyński, Int. J. Mod. Phys. E **19**, 500 (2010).
- [13] K. Siwek-Wilczyńska, T. Cap, M. Kowal, A. Sobiczewski, and J. Wilczyński, Phys. Rev. C **86**, 014611 (2012).
- [14] G. Giardina, G. Fazio, G. Mandaglio, M. Manganaro, A.K. Nasirov, M. V. Romaniuk, Int. J. Phys. Mod. E **19**, 882 (2009).
- [15] G. Giardina, A.K. Nasirov, G. Mandaglio, F. Curciarello, V. De Leo, G. Fazio, M. Manganaro, M. Romaniuk, C. Saccá, Journ. Phys: Conf. Series **282**, 012006 (2011).
- [16] Yu. Ts. Oganessian *et al.*, Phys. Rev. C **74**, 044602 (2006).
- [17] A.K. Nasirov, G. Giardina, A.I. Muminov, W. Scheid and U.T. Yakhshiev, *Proc. Symposium Nuclear Clusters, Ravissholzhausen, Germany*, 5-9 August 2002 (ed. R. V. Jolos and W. Scheid, EP Systema, Debrecen), 415 (2003); Acta Physica Hungarica A **19**, 109 (2004).
- [18] G. Giardina, S. Hofmann, A.I. Muminov, and A.K. Nasirov, Eur. Phys. J. A **8**, 205 (2000).
- [19] G. Fazio, G. Giardina, A. Lamberto, R. Ruggeri, C. Sacca, R. Palamara, A. I. Muminov, A. K. Nasirov, U. T. Yakhshiev, F. Hanappe, T. Materna, and L. Stuttge: J. Phys. Soc. Jpn. **72**, 2509 (2003).
- [20] G.G. Adamian, R.V. Jolos, A.K. Nasirov, A.I. Muminov, Phys. Rev. C **56**, 373 (1997).
- [21] Avazbek Nasirov, Akira Fukushima, Yuka Toyoshima, Yoshihiro Aritomo, Akhtam Muminov, Shuhrat Kalandarov, Ravshanbek Utamuratov, Nucl. Phys. A **759**, 342 (2005).
- [22] S. Raman, C. H. Malarkey, W. T. Milner, C. W. Nestor, Jr., and P. H. Stelson: At. Data Nucl. Data Tables **36**, 1 (1987).
- [23] P. Möller, J.R. Nix, W.D. Myers, and W.J. Swiatecki, At. Data Nucl. Data Tables **59**, 185 (1995).
- [24] C.Y. Wong, Phys. Rev. Lett. **31**, 766 (1973).
- [25] A.B. Migdal, Theory of the Finite Fermi Systems and Properties of Atomic Nuclei, Moscow, Nauka, 1983.
- [26] G.G. Adamian, A.K. Nasirov, N.V. Antonenko, R.V. Jolos, Phys. Part. Nucl. **25**, 583 (1994).
- [27] D. Pines, P. Nozières, Theory of Quantum Liquids, Benjamin, New York, 1966
- [28] G.G. Adamian, N.V. Antonenko, W. Scheid, Nucl. Phys. A **618**, 176 (1997).
- [29] G. Fazio, G. Giardina, G. Mandaglio, F. Hanappe, A. I. Muminov, A. K. Nasirov, W. Scheid, L. Stuttge, Mod. Phys. Lett. A **20**, 391 (2005).
- [30] G. Fazio, G. Giardina, G. Mandaglio, R. Ruggeri, A. I. Muminov, A. K. Nasirov, Yu. Ts. Oganessian, A. G. Popeko, R. N. Sagaidak, A. V. Yeremin, S. Hofmann, F. Hanappe, C. Stodel, Phys. Rev. C **72**, 064614 (14) (2005).
- [31] I. Muntian, Z. Patyk, and A. Sobiczewski, *Phys. of Atomic Nuclei* **66**, 1015 (2003).
- [32] M. Kowal, P. Jachimowicz, and A. Sobiczewski, *Phys. Rev. C* **82**, 014303 (2010).
- [33] P. Möller, A. J. Sierk, T. Ichikawa, A. Iwamoto, R. Bengtsson, H. Uehlenholt, and S. Aberg, Phys. Rev C **79**, 064304 (2009).
- [34] V. I. Zagrebaev, A. V. Karpov and Walter Greiner, Phys. Rev C **85**, 014608 (2012).
- [35] A. K. Nasirov, A. I. Muminov, G. Giardina, G. Mandaglio and M. Manganaro, J. Phys.: Conf. Ser. **205**, 012018 (2010).
- [36] A. K. Nasirov, G. Giardina, G. Mandaglio, M. Manganaro and A. I. Muminov, Int. J. Mod. Phys. E **19**, 997 (2010).